Structural and Functional Effects of Tryptophans Inserted into the Membrane-binding and Substrate-binding Sites of Human Group IIA Phospholipase A_2[†]

Kathleen N. Nemec,[‡] Abhay H. Pande,[‡,||] Shan Qin,[‡,⊥] Ramona J. Bieber Urbauer,[§] Shuhua Tan,[‡,▽] David Moe,[‡,#] and Suren A. Tatulian*[,‡]

Biomolecular Science Center, University of Central Florida, 12722 Research Parkway, Orlando, Florida 32826, and Department of Biochemistry and Molecular Biology, University of Georgia, 120 Green Street, Davison Life Sciences Complex, Athens, Georgia 30602

Received July 17, 2006

ABSTRACT: Phospholipase A_2 (PLA_2) enzymes become activated by binding to biological membranes and hydrolyze phospholipids to free fatty acids and lyso-phospholipids, the precursors of inflammatory mediators. To understand the functional significance of amino acid residues at key positions, we have studied the effects of the substitution of Val^3 (membrane binding surface) and Phe^5 (substrate binding pocket) of human group IIA PLA_2 by tryptophan on the structure and function of the enzyme. Despite the close proximity of the sites of mutations, the V3W mutation results in substantial enhancement of the enzyme activity, whereas the F5W mutant demonstrates significantly suppressed activity. A structural analysis of all three proteins free in buffer and bound to membranes indicates that large differences in activities result from distinct conformational changes in PLA_2s upon membrane binding. Although PLA_2 and the V3W mutant demonstrate a decrease in helical content and an increase in helix flexibility, the F5W mutant experiences partial distortion of the α-helical structure presumably resulting from the tendency of Trp^5 to insert into the membrane. Furthermore, whereas the PLA_2 and the V3W mutant bind to the membrane at similar and apparently productive-mode orientation, the F5W mutant binds to membranes with a distinctly different orientation. It is suggested that both the stimulatory effect of the V3W mutation and the inhibitory effect of the F5W mutation result from the high affinity of Trp for the membrane−water interface. Although Trp^3 at the membrane binding face of PLA_2 facilitates the proper membrane binding of the enzyme, Trp^5 in the internal substrate binding site causes partial unwinding of the *N*-terminal helix in order to interact with the membrane.

Enzymes of the phospholipase A_2 (PLA_2)[1] family hydrolyze the *sn*-2 ester bond of glycerophospholipids and are involved in physiological activities ranging from dietary lipid digestion to inflammation, allergy, and tumorigenesis through lipid-derived mediators such as eicosanoids and platelet activating factor (*1*−*5*). Certain mammalian isoforms of secretory PLA_2s demonstrate antibacterial activity (*6*, *7*) and participate in lipoprotein-mediated atherosclerosis (*8*), whereas snake venom PLA_2s exert a myotoxic effect that may involve interactions with growth factor receptors (*9*, *10*).

PLA_2s belong to the class of interfacial enzymes that undergo a dramatic increase in activity upon binding to phospholipid membranes or micelles (*11*, *12*). Group IB PLA_2s demonstrate reasonable hydrolytic activity toward zwitterionic phosphatidylcholine (PC) membranes (*13*−*15*), whereas group IIA PLA_2s show appreciable membrane binding and activity only when the membranes contain >15 mol % acidic lipid (*16*, *17*). Such functional features are apparently determined by the primary and the 3-D structures of PLA_2s as well as their pI values and excess charge (*11*, *12*, *18*−*20*). The *N*-terminal amphipathic α-helix of group I/II PLA_2s significantly contributes to the enzyme function by providing key residues for surface binding and by facilitating phospholipid entrance into the hydrophobic substrate-binding pocket (*19*−*24*). Group IB enzymes contain

[†] This work was supported by National Institutes of Health Grant HL65524.

* To whom correspondence should be addressed. Tel: 407-882-2260. Fax: 407-384-2062. E-mail: statulia@mail.ucf.edu.

[‡] University of Central Florida.

[§] University of Georgia.

[||] Present address: Biological Science Group, Birla Institute of Technology and Science, Pilani, India 333031.

[⊥] Present address: Division of Nephrology, Children's Hospital Boston, and Department of Pediatrics, Harvard Medical School, Boston, MA 02115.

[▽] Present address: 7032 Durham Research Center, University of Nebraska Medical Center, 985870 Nebraska Medical Center, Omaha, NE 68198.

[#] Present address: VaxDesign Corp., 2721 Discovery Drive, Central Florida Research Park, Orlando, FL 32826.

[1] Abbreviations: ATR, attenuated total reflection; bisPy-PC, 1,2-bis-(1-pyrenedecanoyl)-*sn*-glycero-3-phosphocholine; CD, circular dichroism; DHTPC, diheptanoyl thiophosphatidylcholine; DPPC, 1,2-dipalmitoyl-*sn*-glycero-3-phosphocholine; FPE, *N*-(fluorescein-5-thiocarbamoyl)-1,2-dihexadecanoyl-*sn*-glycero-3-phosphoethanolamine; FTIR, Fourier transform infrared; $hIIAPLA_2$, human group IIA phospholipase A_2; HX, hydrogen/deuterium exchange; LUV, large unilamellar vesicle; PC, phosphatidylcholine; PLA_2, phospholipase A_2; POPC, 1-palmitoyl-2-oleoyl-*sn*-glycero-3-phosphocholine; POPG, and 1-palmitoyl-2-oleoyl-*sn*-glycero-3-phosphoglycerol; PS, phosphatidylserine.

10.1021/bi061440r CCC: $33.50
Published on Web 09/21/2006

a unique Trp^3 residue, which is conserved across species and determines the ability of PLA_2 to bind to and hydrolyze PC membranes. The third position of other PLA_2 isoforms is occupied by aromatic or hydrophobic residues, such as Tyr, Phe, Val, Leu, or Ile. Although these residues might support the binding of respective PLA_2s to zwitterionic membranes by means of hydrophobic interactions, they are not as effective as Trp, which is now recognized as a mediator of protein−membrane interactions (*25*, *26*). The only other known case of the occurrence of Trp in the *N*-terminal helix is Trp^6 in certain snake venom PLA_2s (*27*−*29*).

While the cationic residues of the *N*-terminal helix contribute to the electrostatic component of the membrane binding of group I/II PLA_2s, residues at positions 3 and 5 seem to be crucial for nonelectrostatic membrane binding and substrate binding, respectively. The mutation of Trp^3 of bovine group IB PLA_2 with Ala caused a 3−7-fold decrease in activity of the enzyme toward dimyristoylphosphatidylmethanol membranes or diheptanoyl-PC micelles (*20*), whereas the replacement of Val^3 of human group IIA PLA_2 with Trp substantially increased its capability to bind to and hydrolyze PC membranes (*16*, *30*, *31*). Interestingly, Trp mutations of the other seven nonpolar residues that constitute the hydrophobic membrane-binding surface of PLA_2 had either no or smaller stimulatory effects compared to that of the V3W mutant (*31*).

The substrate-binding face of the *N*-terminal helix is lined with strongly hydrophobic residues at the 2-, 5-, and 9-positions, with an invariant Phe at position 5. Atomic resolution structures of group I and II PLA_2s with bound inhibitors indicate intimate van der Waals contacts between the side chain of Phe^5 and the hydrophobic moieties of the inhibitor (*32*−*35*). The tight contact between Phe^5 and the substrate appears to be critical to the function of PLA_2s because replacement of Phe^5 by either hydrophobic or aromatic residues, smaller or larger in size, strongly inhibit the activity of bovine IB PLA_2 (*20*, *21*). These findings suggest that Phe^5 may serve to facilitate a productive phospholipid−PLA_2 interaction, at least for group IB enzymes.

These studies clearly underscore the functional importance of Trp^3 and Phe^5. The enhanced activity of the V3W mutant of human group IIA PLA_2 ($hIIAPLA_2$) against PC membranes was interpreted in terms of Trp-mediated stronger membrane binding of PLA_2 (*30*, *31*). It is interesting, however, to see how this mutation affects the enzyme activity against short-chain phospholipid micelles when the monodisperse lipid can efficiently compete with that in the micellar form. Also, the functional roles of the hydrophobic residues at the substrate-binding face of the *N*-terminal helix of group II PLA_2s, most importantly Phe^5, have not been addressed by means of mutagenesis. Furthermore, structural aspects of interfacial activation of PLA_2s and the effects of mutations at the membrane- or substrate-binding sites have not been studied systematically. Therefore, in this work, we have studied the effects of V3W and F5W mutations in $hIIAPLA_2$ on the structure and activity of the enzyme, using activity assays and a variety of biophysical approaches. Our data indicate a strong increase in the activity of the V3W mutant and substantial inhibition of the F5W mutant toward phospholipid micelles and membranes. Structural studies show that the $hIIAPLA_2$ and the V3W mutant undergo an increase in conformational flexibility upon membrane binding, but the F5W mutant experiences significant perturbation of the structure and dynamics and binds to the membrane with a distinctly different orientation. The data indicate that single Trp mutations at closely located sites have dramatically different effects on the structure and function of the enzyme and open new opportunities for the regulation of enzyme function by site-directed mutagenesis.

MATERIALS AND METHODS

Materials. Miniprep and PCR purification kits were obtained from Qiagen (Valencia, CA). Designed primers for point mutation were from Molecula (Herndon, VA), pGEM-T vectors and DH5α bacteria were from Novagen (Madison, WI), and restriction enzymes were from Amersham (Piscataway, NJ). The $sPLA_2$ activity kit was from Cayman Chemical (Ann Arbor, MI). The $hIIAPLA_2$ synthetic gene inserted in a pET11a vector was kindly provided by Professor David C. Wilton (University of Southampton, U.K.). The PLA_2 sequence incorporates a N1A mutation in order to facilitate the removal of the initiator methionine in *E. coli*. Because the structure and activity of the N1A mutant of $hIIAPLA_2$ are nearly identical to those of the wild-type enzyme (*22*), in the forthcoming text, we will refer to the enzyme as $hIIAPLA_2$. Correspondingly, the two Trp mutants will be designated V3W and F5W. The lipids 1-palmitoyl-2-oleoyl-*sn*-glycero-3-phosphocholine (POPC) and 1-palmitoyl-2-oleoyl-*sn*-glycero-3-phosphoglycerol (POPG) were purchased from Avanti Polar Lipids (Alabaster, AL), 1,2-bis-(1-pyrenedecanoyl)-*sn*-glycero-3-phosphocholine (bisPy-PC) was from Molecular Probes (Eugene, OR), and *N*-(fluorescein-5-thiocarbamoyl)-1,2-dihexadecanoyl-*sn*-glycero-3-phosphoethanolamine (FPE) was from Invitrogen Corp. (Carlsbad, CA). Most of the other chemicals were obtained from Sigma-Aldrich Co. (St. Louis, MO).

Production of Recombinant Proteins. The expression plasmid pET11a-N1A containing the gene of $hIIAPLA_2$, which incorporates an N1A mutation, was used as a template for the production of the V3W and F5W mutants. The mutated genes were generated by PCR, using the following forward primers: 5′-TACAT ATG GCC CTG TGG AAC TTC CAC CGT ATG-3′ for V3W and 5′-TACAT ATG GCC CTG GTA AAC TGG CAC CGT ATG-3′ for F5W (mutated codons are underlined). The same reverse primer was used for both constructs: 5′-TCA TCG ATA AGC TTC ACT ATT AGC-3′. The PCR product was cloned into a pGEM-T vector and was sequenced using a Beckman-Coulter CEQ 2000 XL DNA sequencer (Fullerton, CA). Each mutated PLA_2 gene sequence was subcloned into pET21a(+) using the *Nde*I/*Hin*dIII sites. The pET11a-N1A and the pET21a-(+) plasmids harboring the V3W and the F5W mutated genes were electroporated into *E. coli* DH5α and amplified, using standard procedures. A positive clone of each of the three constructs, as identified by sequencing, was placed in *E. coli* BL21(DE3) for T7-driven expression. The proteins were expressed and purified using a protocol described previously (*22*) and modified to optimize the yield and the purity of PLA_2. All proteins were expressed as inclusion bodies and were denatured and refolded using standard procedures (*23*). Because of the strong tendency of $hIIAPLA_2$ to adsorb to surfaces, all glassware, plastic tips, and tubes were first coated with Sigmacote (Sigma-Aldrich Co.) to reduce the

loss of protein by binding to contact surfaces. The bacterial cell lysis buffer was supplemented with 0.2 mg/mL lysozyme in order to enhance cell lysis and maximize the yield of the protein. An important modification of hIIAPLA$_2$ purification was the use of a HiLoad Superdex 75 size-exclusion column (Amersham) following initial protein purification with a Heparin column. This yielded highly pure and active hIIAPLA$_2$. The V3W and F5W mutants were expressed and purified using the same procedures. All proteins have been lyophilized from pure water and kept at −80 °C, under which conditions the structural features and the enzymatic activity were maintained for at least several months.

PLA$_2$ Activity Assays. The activity of PLA$_2$ was measured using two different assays. The enzyme activity against diheptanoyl thiophosphatidylcholine (DHTPC) micelles was measured using a sPLA$_2$ activity kit from Cayman Chemical, as described earlier (*23*). The activity was also measured against large unilamellar vesicles (LUVs), which were prepared by extrusion through 100 nm pore-size polycarbonate membranes using a Liposofast extruder (Avestin, Ottawa, Canada). This assay was carried out in a buffer containing 50 mM NaCl, 2.2 mM $CaCl_2$, and 50 mM Hepes at pH 7.5, using phospholipid vesicles of desired lipid composition and containing 5 mol % bisPy-PC, at a total lipid concentration of 0.5 mM. The reaction was initiated by adding PLA$_2$. The pyrene moiety of bisPy-PC was excited at 347 nm, and emission spectra were recorded between 370 and 490 nm. The emission spectrum of monomeric pyrene contains two peaks at 380 and 396 nm, whereas the close proximity of pyrene moieties results in a strong excimer peak at 470 nm (*19*, *36*). As PLA$_2$ hydrolyzes the bisPy-PC, the free fatty acid and the lysolipid, each of which has a pyrene moiety, separate from each other, resulting in a decrease in the excimer signal at 470 nm and an increase in the monomer signal at 380 nm. This allows the determination of activity as $R_t/R_0 - 1$, where R_t is the ratio of fluorescence intensities at 380 and 470 nm at time t, $R_t = (F_{380}/F_{470})_t$, and R_0 is R_t before the addition of PLA$_2$.

Concentrations of all proteins were determined using the respective extinction coefficients at 280 nm (ϵ_{280}), which were determined by weighing 1 mg of the protein, preparing a protein solution of precisely known concentration, and measuring the absorption at 280 nm, using a 4 mm path-length quartz cuvette and a Cary 100 spectrophotometer (Varian Inc., Palo Alto, CA).

Membrane Binding Experiments. Binding of PLA$_2$ to vesicle membranes was measured on the basis of an increase in fluorescence emission intensity of FPE in membranes of LUVs upon protein binding, as described previously (*19*, *37*, *38*). In brief, FPE was incorporated at 2 mol % into POPC/POPG (3:2) vesicles, which were prepared as described above. Total lipid concentration was $[L] = 0.175$ mM, in a buffer of 10 mM Hepes, 1 mM NaN_3, and 1 mM EGTA at pH 7.4. Fluorescence spectra were measured using a J-810 spectrofluoropolarimeter (Jasco Co., Tokyo, Japan). This instrument is a spectropolarimeter equipped with a Peltier temperature controller and an additional photomultiplier tube mounted at 90°, which can be used for fluorescence or light-scattering measurements in addition to circular dichroism (CD) measurements (*19*, *23*, *39*). Excitation was at 490 nm, and emission spectra were recorded between 500 and 540 nm at 25 °C, using a 4 × 4 mm^2 rectangular quartz cuvette. Excitation and emission slits were 4 and 10 nm, respectively. After recording an initial spectrum of vesicles in the buffer, the protein was added to the lipid suspension at increasing concentrations from a stock solution. After each consecutive addition, the suspension was allowed to equilibrate for 2 min with constant stirring before fluorescence emission spectra were collected. Changes in the peak fluorescence intensity, ΔF, were determined for each protein concentration, $[P]$. In control experiments, similar volumes of the buffer were added instead of the protein solution in order to correct the values of ΔF for the dilution effect. The corrected values of ΔF were plotted as a function of $\Delta F/[P]$ in order to obtain Scatchard plots. The extrapolated intercept with the ΔF axis and the slope of the Scatchard plots were used to evaluate two parameters, the maximum value of ΔF at saturating protein concentration, ΔF_{max}, and the protein concentration corresponding to half saturation, $[P]_{1/2}$. The experimental binding isotherms were constructed by plotting $\Delta F_{rel} \equiv \Delta F/\Delta F_{max}$ as a function of $[P]$. Theoretical binding isotherms were obtained using a previously derived equation (*19*)

$$\Delta F_{rel} = a - \sqrt{a^2 - \frac{N[P]}{\delta[L]}} \quad (1)$$

where

$$a = \frac{1}{2}\left(\frac{N(K_D + [P])}{\delta[L]} + 1\right) \quad (2)$$

In eqs 1 and 2, K_D is the dissociation constant, N is the number of lipid molecules corresponding to a protein binding site (i.e., the number of lipids that become inaccessible for protein binding upon binding of each protein molecule), and δ is the total fraction of lipids accessible to protein binding. It can be shown (*19*) that at half-saturation of protein binding the following relationship holds.

$$K_D = [P]_{1/2} - \frac{\delta[L]}{2N} \quad (3)$$

Because $[P]_{1/2}$ can be determined on the basis of experimental binding data, as described above, and under conditions when the protein is added to preformed 100 nm unilamellar vesicles, $\delta = 0.52$ (*19*), eq 3 represents an explicit relationship between K_D and N. This means that eqs 1−3 can be combined (by inserting the expression for K_D from eq 3 into eq 2 and then inserting a into eq 1) to obtain a binding isotherm that contains only one unknown, N. This isotherm was used to fit the experimental binding data, and N was varied until a best fit was obtained. Then, the best fit value of N was used to determine K_D through eq 3.

Fluorescence and Circular Dichroism Experiments. Fluorescence and CD measurements were conducted using the J-810 spectrofluoropolarimeter, described above. For CD experiments, the proteins were dissolved in 10 mM Na-phosphate buffer at pH 7.4, at a concentration of 0.1 mg/mL, and measurements were conducted using a 0.2 mm optical path-length quartz cell. Ten scans were collected between 260 and 180 nm, which were averaged and corrected for background by subtracting the buffer spectra. Mean residue molar ellipticities $[\theta]$ were calculated as described earlier (*23*).

FTIR Experiments. Fourier transform infrared (FTIR) experiments were carried out using a Vector 22 FTIR spectrometer (Bruker Optics, Billerica, MA), as described previously (*23*). For direct transmission experiments, the protein, lyophilized from pure H_2O, was dissolved in a D_2O-based buffer containing 100 mM NaCl, 1mM NaN_3, 1 mM EGTA, and 50 mM Hepes (pH* 7.0, which is equivalent to pH 7.4 after correction for the isotope effect) and was immediately assembled between two CaF_2 windows, using a 25 μm Teflon spacer, and consecutive spectra were recorded for 1 h. Spectra of the protein dissolved in a H_2O-based buffer were also recorded, using a 6 μm spacer. For attenuated total reflection Fourier transform infrared (ATR-FTIR) experiments, a model 611 Langmuir−Blodgett trough (Nima, Coventry, U.K.) was used to deposit a POPC monolayer on a germanium internal reflection plate (Spectral Systems, Irvington, NY). The plate with the monolayer was assembled into an ATR flow cell, and sonicated POPC/POPG (7:3, mol/mol) vesicles were injected to form supported phospholipid bilayers. Excess lipid was removed by flushing with buffer. The protein in a H_2O-based buffer containing 100 mM NaCl, 1mM NaN_3, 1 mM EGTA, and 50 mM Hepes (pH 7.4) was then injected into the ATR cell and permitted to adsorb to the membrane for 15 min, followed by gently flushing with a D_2O-based buffer of the same composition. Spectra were collected at parallel and perpendicular polarizations of the incident infrared light at varying time points for 1 h. For both direct transmission and ATR-FTIR measurements, time of deuteration of the protein amide hydrogens was counted starting at first exposure of the protein to D_2O. All spectra were processed and analyzed using a Grams/AI V7 software suite (ThermoGalactic, Salem, NH). For evaluation of the protein secondary structure and kinetics of hydrogen/deuterium exchange (HX), polarized spectra were first corrected in order to obtain polarization-independent spectra, $A = A_{||} + 0.8A_{\perp}$, as described previously (*40*, *41*). Components of amide I and amide II bands of FTIR spectra were identified by curve-fitting, using the number and positions of the peaks in the inverted second derivative spectra. The results of curve-fitting were considered satisfactory when the peak frequencies of all components were within a ± 1 cm^{-1} range compared to the input frequencies and when the sum of all components was coincident to the measured spectrum. The kinetics of HX was determined on the basis of the time-dependent decrease in the amide II band intensity around 1545 cm^{-1}, as previously described (*41*, *42*). The fraction of unexchanged amide protons at time t was presented as $[H/(H + D)]_t$, where H and D are the numbers of unexchanged and exchanged backbone amide groups. The time dependence of HX was presented as follows.

$$\left(\frac{H}{H+D}\right)_t = \frac{A_{\text{amideII,t}}}{A_{\text{amideII,0}}} = a_0 + a_1 e^{-k_1 t} + a_2 e^{-k_2 t} \quad (4)$$

In eq 4, $A_{\text{amideII,0}}$ and $A_{\text{amideII,t}}$ are the integrated amide II band intensities at time 0 (before exposure to D_2O) and at time t of exposure to D_2O. To eliminate the effects of possible changes in the overall signal, for example, due to protein adsorption or desorption, $A_{\text{amideII,0}}$ and $A_{\text{amideII,t}}$ were normalized by dividing by the amide I areas at corresponding time points. The parameters a_0, a_1, and a_2 in eq 4 are the fractions of exchange-resistant, slow-exchanging, and fast-exchanging residues, and k_1 and k_2 are the rate constants of slow- and fast-exchanging residues, respectively. Thus, this approach classifies all backbone amide groups of the protein into three kinetic populations, as described above. Although this may be considered an oversimplification, attempts to deduce more detailed information on the HX kinetics based on the time-dependent decrease in the amide II band intensity would be increasingly unreliable (*41*). The current approach provides a reasonable number of parameters that can reliably describe changes in the protein dynamic structure upon amino acid mutations or membrane binding.

RESULTS AND DISCUSSION

Mutation, Expression, and Purification of hIIAPLA$_2$. Incorporation of tryptophan codons into the 3rd or 5th positions of the two mutated hIIAPLA$_2$ genes was confirmed by DNA sequencing (not shown). The yields of purified hIIAPLA$_2$, the V3W mutant, and the F5W mutant were approximately 30, 5, and 25 mg per liter of *E. coli* cell culture, respectively. Siliconization of all surfaces that come into contact with the protein (tubes, pipet tips, etc.) significantly increased the yield of proteins by preventing nonspecific adsorption to the surfaces. The extinction coefficients of all three proteins were measured by a straightforward method (see above) and were 10,338 M^{-1} cm^{-1} for hIIAPLA$_2$, 11,416 M^{-1} cm^{-1} for V3W, and 15,486 M^{-1} cm^{-1} for F5W. The highly pure protein samples, which were required for biophysical analysis, were obtained by HiLoad Superdex 75 size-exclusion column chromatography, following the initial purification by a Heparin column. The profile of elution of hIIAPLA$_2$ from the Superdex size-exclusion column showed two protein peaks with similar molecular weights, one with negligible PLA_2 activity and the other, corresponding to longer retention times, with profoundly high PLA_2 activity (Figure 1). The elution profile of the V3W mutant was similar to that of hIIAPLA$_2$ and was slightly shifted toward longer retention times, whereas the F5W mutant eluted as a broader single peak corresponding to the retention time of the active fraction of hIIAPLA$_2$ (not shown). For hIIAPLA$_2$ and the V3W mutant, only the highly active fractions were collected, whereas for the F5W mutant, the central part of the single elution peak was collected, dialyzed against pure water, lyophilized, and stored at −80 °C.

Activities of hIIAPLA$_2$ and the Tryptophan Mutants. Comparison of the activities of the three proteins toward DHTPC micelles indicated a 4-fold increase in activity of the V3W mutant compared to that of hIIAPLA$_2$, whereas the F5W mutant had negligibly low activity (Figure 2). The activities of PLA_2s were also assayed against LUVs labeled with bisPy-PC. Figure 3A shows representative fluorescence spectra that indicate a time-dependent decrease in the pyrene excimer emission intensity at 470 nm and a parallel increase in the monomer signal at 380 nm following the addition of hIIAPLA$_2$ to LUVs composed of 55, 40, and 5 mol % of POPC, POPG, and bisPy-PC, respectively. The activities of the hIIAPLA$_2$ and the two mutants were measured for pure zwitterionic 1,2-dipalmitoyl-*sn*-glycero-3-phosphocholine (DPPC) membranes and for membranes containing POPC with various fractions of an anionic lipid, POPG. In the case of DPPC LUVs, no activity of hIIAPLA$_2$ could be detected at 25 °C for at least 1 h following PLA_2 addition. However,

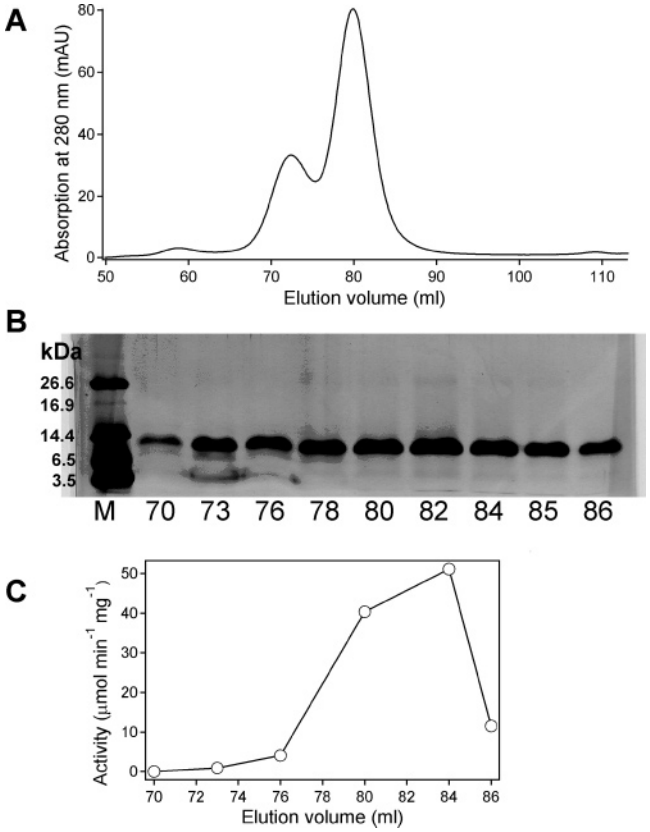

FIGURE 1: Elution profile from HiLoad Superdex 75 size-exclusion column (A), silver-stained SDS-polyacrylamide gel (B), and the activity profile of hIIAPLA$_2$ across the elution fractions (C). The second major elution peak is characterized by high purity and activity. In panel B, M stands for marker and is followed by elution volumes in mL. In panel C, the activity against DHTPC micelles is measured using the Cayman sPLA$_2$ kit as described in Materials and Methods.

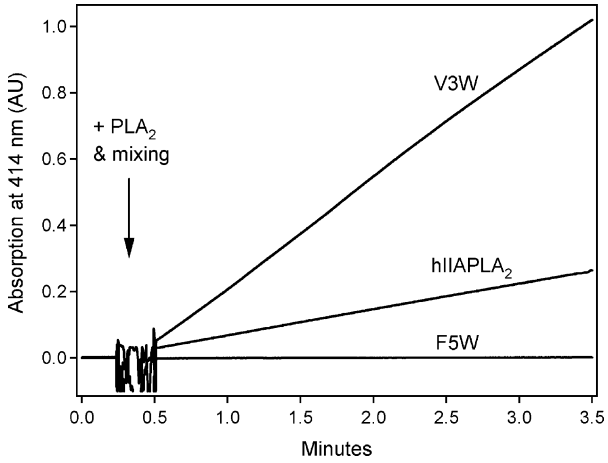

FIGURE 2: Activities of hIIAPLA$_2$, the V3W mutant, and the F5W mutant, as indicated, against DHTPC micelles obtained using a sPLA$_2$ activity kit from Cayman Chemical. The assay buffer contained 100 mM KCl, 10 mM $CaCl_2$, 0.3 mM Triton X-100, 1 mg/mL bovine serum albumin, 25 mM Tris-HCl (pH 7.5), 1.5 mM DHTPC, and 0.4 mM 5,5′-dithio-bis-(2-nitrobenzoic acid). Activity is determined by an increase in absorbance at 414 nm, which is generated by cleavage of 5,5′-dithio-bis-(2-nitrobenzoic acid) into 5-thio-nitrobenzoic acid upon hydrolysis of the *sn*-2 chain of DHTPC by PLA$_2$ and exposure of free thiols. Specific activities for each protein, determined using an extinction coefficient for 5-thio-nitrobenzoic acid $\epsilon_{414} = 13{,}600\ M^{-1}\ cm^{-1}$, were 45, 185, and 0.0001 μmol/min/mg for hIIAPLA$_2$, V3W, and F5W, respectively.

when the temperature approached the gel-to-liquid-crystal phase transition temperature of DPPC (T_m = 41.5 °C), enzyme activity could be measured with a complex kinetic feature depending on the particular temperature. At 38 °C, after the addition of hIIAPLA$_2$, there was an ~5 min lag period, followed by an intermediate activity, which was followed by the onset of high activity at 15−17 min (Figure 3B). Interestingly, the V3W mutant showed a brief (2−3 min) intermediate activity followed by very high activity, without a measurable lag time, and the F5W barely showed any activity (Figure 3B). Experiments at temperatures higher than T_m were not conducted in order to avoid possible thermal effects on the protein structure. Qualitatively different results were obtained with POPC/POPG (80:15, mol/mol) membranes. In this case, the V3W mutant of PLA$_2$ demonstrated very high activity immediately, the hIIAPLA$_2$ had a 1.5-min lag, followed by activation to a level of ~3% of the activity of the V3W mutant, and the F5W mutant showed a lag period and a subsequent moderate activity, about half that of hIIAPLA$_2$ (Figure 3C).

Our data are consistent with earlier findings that group IIA PLA$_2$ shows little activity against PC membranes in the gel phase ($T \ll T_m$) but becomes active near T_m (*43*, *44*). Under certain conditions, for example, for zwitterionic PC membranes, PLA$_2$ activity was preceded by a lag phase, which was interpreted in terms of gradual accumulation of the reaction products in the membrane leading to the onset of high activity (*16*, *43*, *44*). The lag was shown to become shorter or to disappear with increasing fractions of anionic lipids (*16*, *45*), also in agreement with our data shown in Figure 3B and C.

Earlier studies revealed a significant (30-fold) increase in the activity of hIIAPLA$_2$ against multilamellar PC membranes upon a V3W mutation, but little change in activity when anionic POPG vesicles were used as substrate (*31*). However, the V3W mutation caused a reduction of the lag time from 6 to 1 min for the activation of hIIAPLA$_2$ against POPC LUVs, followed by a subsequent 2-fold higher activity (*16*). In this latter study, the activity of the V3W mutant was approximately two times higher than that of the hIIAPLA$_2$ against POPG vesicles but was lower against vesicles composed of PC and phosphatidylserine (PS) (4:1, mol/mol). These findings indicate a complex effect of the V3W mutation on the behavior of hIIAPLA$_2$ toward zwitterionic and anionic membranes. Although the F5W mutation of hIIAPLA$_2$ has not been reported, to the best of our knowledge, the replacement of Phe^5 of bovine pancreatic PLA$_2$ by smaller or larger residues, such as Ala, Val, Tyr, Trp, resulted in substantial inhibition of the enzyme against both phospholipid micelles and vesicles (*20*, *21*). Thus, our data presented in Figures 2 and 3 are in general agreement with earlier findings and provide new and interesting results indicating dramatically different effects of the insertion of Trp into two very closely located sites of hIIAPLA$_2$ on enzyme activity. Also, we uncover significant differences in the effects of V3W and F5W mutations on the activity of hIIAPLA$_2$ against zwitterionic micelles, zwitterionic membranes, and anionic membranes. In particular, we detected a nearly complete loss of hIIAPLA$_2$ activity against PC micelles and membranes upon F5W mutation but a retention

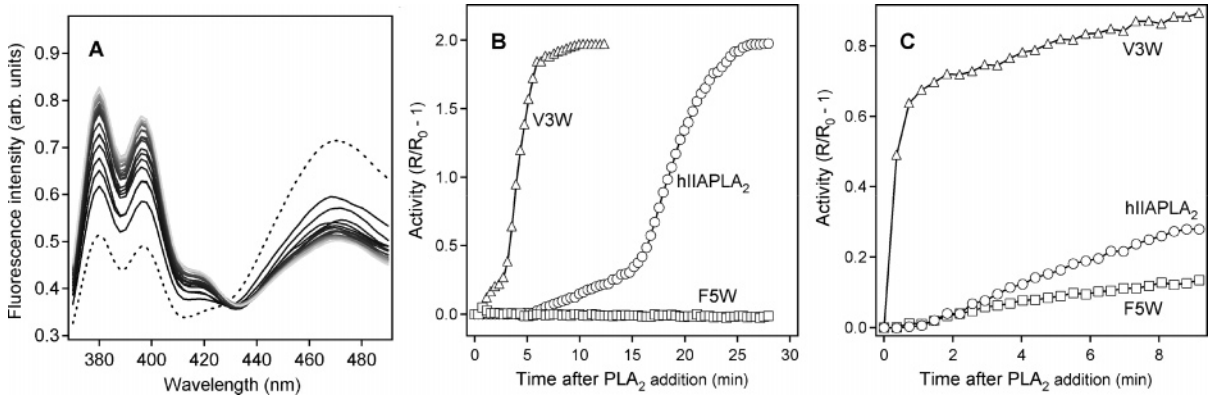

FIGURE 3: PLA_2 activity against large unilamellar vesicles, as measured by the bisPy-PC method. (A) Fluorescence spectra of LUVs containing POPC, POPG, and bisPy-PC (55, 40, and 5 mol %, respectively), before (---) and after the addition of 2.6 μM hIIAPLA$_2$; decreasing darkness of solid lines corresponds to the progression of time following PLA_2 addition. Excitation was at 347 nm, and the temperature was 25 °C. (B) Kinetics of hydrolysis of DPPC LUVs containing 5 mol % bisPy-PC by 1.8 μM hIIAPLA$_2$ and the two mutants, as indicated, at 38 °C. (C) Hydrolysis of LUVs composed of 80 mol % POPC, 15 mol % POPG, and 5 mol % bisPy-PC by 2.7 μM hIIAPLA$_2$ and the two mutants, as indicated, at 25 °C. In all cases, the buffer contained 50 mM NaCl, 2.2 mM $CaCl_2$, and 50 mM HEPES at pH 7.4. The total lipid concentration was 0.5 mM.

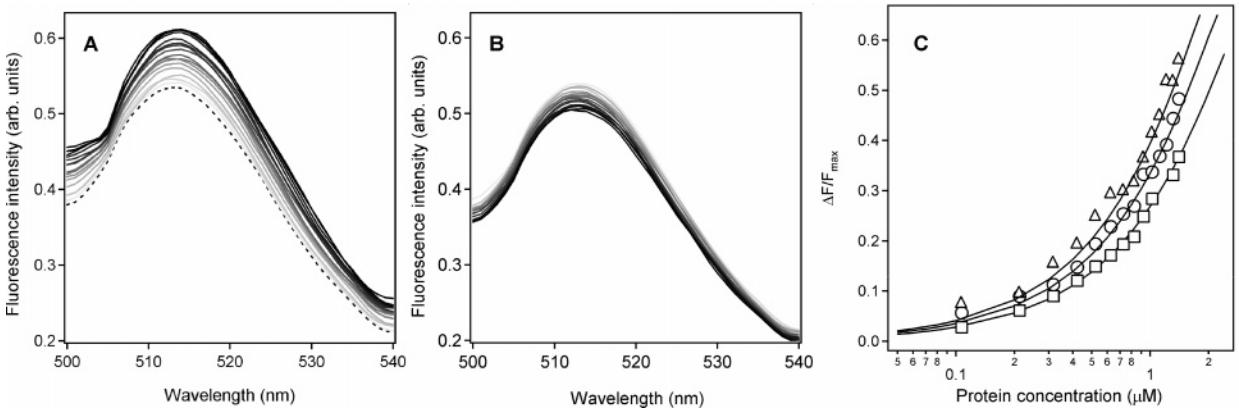

FIGURE 4: (A) Fluorescence spectra of LUVs composed of 58 mol % POPC, 40 mol % POPG, and 2 mol % FPE without (---) and with increasing concentrations of hIIAPLA$_2$ (increasing darkness of solid lines). (B) Change in the fluorescence spectra of LUVs of lipid composition identical to that in A, diluted by adding the same volumes of buffer without the protein. Sample dilution is reflected in decreasing fluorescence intensity (increasing darkness of the solid lines). Excitation was at 490 nm. (C) Isotherms of binding of hIIAPLA$_2$ (○), the V3W (△), and the F5W (□) to membranes of LUVs with lipid composition as specified above. The lines are constructed through eq 1, using the following binding parameters: $K_D = 0.3$ μM, $N = 36$ for hIIAPLA$_2$; $K_D = 0.19$ μM, $N = 41$ for the V3W mutant; and $K_D = 0.5$ μM, $N = 30$ for the F5W mutant. The buffer was 1 mM NaN_3, 1 mM EGTA, and 10 mM Hepes at pH 7.4, and the temperature was 25 °C.

of significant activity against anionic membranes, which is further discussed below.

Membrane Binding of hIIAPLA$_2$ and the Tryptophan Mutants. The above data raise several questions. What is the reason for increased activity of the V3W mutant and suppressed activity of the F5W mutant compared to that of hIIAPLA$_2$? Why does the F5W mutant have little activity toward DHTPC micelles and DPPC vesicles but retain appreciable activity toward negatively charged POPC/POPG vesicles? In an attempt to answer these questions, we have analyzed the membrane binding properties and structural features of free and membrane-bound hIIAPLA$_2$ and the two mutants.

The measurement of the membrane binding of hIIAPLA$_2$ is not a simple task because the protein does not bind to zwitterionic membranes, and conversely, binding to anionic membranes is very strong and causes the formation of conglomerates containing multiple protein−vesicles complexes due to the highly cationic nature of the protein (*16*, *31*, *46*, *47*). Vesicle aggregation can be minimized by different strategies, such as by using a high ionic strength buffer, membranes with moderate fractions of anionic lipids, or appropriate protein/lipid molar ratios. In membrane binding experiments, we have used membranes composed of 58 mol % zwitterionic and 40 mol % anionic lipids, plus 2 mol % fluorescein-labeled FPE, at a relatively low total lipid concentration of 175 μM. The protein concentration was only increased to levels that resulted in significant changes in the FPE fluorescence signal in order to reliably measure membrane binding (Figure 4A) and but did not cause significant vesicle aggregation. As described in Materials and Methods, the parameters K_D and N were not chosen randomly during the construction of the best-fit theoretical isotherms; they are strictly related to each other through eq 3. The theoretical binding isotherms, given by eq 1, were constructed by varying only one parameter, N, until the best fit with the experiment was achieved. Then, the corresponding values for K_D were derived from eq 3. A satisfactory description of the experimental data could be achieved using the binding parameters that vary within certain limits:

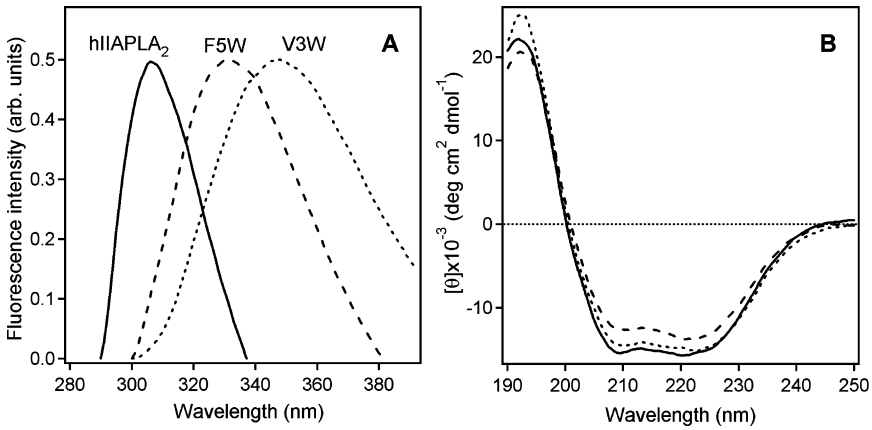

FIGURE 5: (A) Fluorescence spectra of the hIIAPLA$_2$ and the two mutants, as indicated. In the case of the V3W and F5W mutants, Trp fluorescence was measured using excitation at 290 nm, whereas in the case of hIIAPLA$_2$, Tyr fluorescence was measured using excitation at 275 nm. In all cases, the 4 μM protein sample was in a buffer of 1 mM EGTA and 10 mM Hepes at pH 7.4, contained in a 4 × 4 mm^2 rectangular quartz cuvette. The peak intensities of the fluorescence spectra are normalized to the same height for easier assessment of the spectral shift. (B) Far-UV CD spectra of the hIIAPLA$_2$ and the two mutants, as indicated, in a buffer of 10 mM Na-phosphate buffer at pH 7.4. The samples were contained in a 0.2 mm flat quartz cuvette. Protein concentrations were 7 μM, and the temperature was 25 °C. The spectra have been averaged using the data of three independent experiments. The correspondence between different types of lines and PLA$_2$ molecules is the same as that in panel A.

$K_D = 0.3 \pm 0.13$ μM, $N = 36 \pm 4$ for hIIAPLA$_2$, $K_D = 0.19 \pm 0.08$ μM, $N = 41 \pm 3$ for the V3W mutant, and $K_D = 0.5 \pm 0.22$ μM, $N = 30 \pm 5$ for the F5W mutant. The data presented in Figure 4C are described using theoretical isotherms corresponding to the mean values of K_D and N. Although the data of independent experiments consistently showed that affinities of binding to anionic membranes of the three proteins are arranged in the sequence V3W > hIIAPLA$_2$ > F5W, the differences in K_D values were not significant. Also, this procedure yields slightly different values of N for the three proteins, but they are still within a reasonable range of 30−40 lipids per membrane-bound PLA$_2$ molecule and are in good agreement with earlier data (*17*, *19*, *23*, *48*).

Our results of the poor binding of hIIAPLA$_2$ to zwitterionic membranes and the strong binding to anionic membranes indicate a significant electrostatic component in PLA$_2$−membrane interactions, consistent with data obtained previously (*23*, *31*, *46*, *47*, *49*). The dissociation constant of hIIAPLA$_2$ for membranes containing 40 mol % POPG ($K_D = 0.3$ μM) is in good agreement with earlier results obtained under similar conditions (*19*). Beers et al. (*31*) used the sucrose-loaded vesicle centrifugation method to show that hIIAPLA$_2$ did not bind to PC or even PC/PS (82:18, mol/mol) membranes, but V3W did bind to latter membranes with $K_D = 0.21$ mM. However, Bezzine et al. (*16*) detected a nearly 100-fold stronger binding (in terms of K_D) of the V3W mutant to membranes composed of 80 mol % PC and 20 mol % PS compared to that of hIIAPLA$_2$ ($K_D = 2.6$ μM for the V3W vs 230 μM for the hIIAPLA$_2$). Our data show only a 2-fold stronger binding affinity of the V3W mutant for anionic membranes compared to that of hIIAPLA$_2$. Despite large quantitative differences in the absolute values of binding constants, which likely result from differences in methods used and the experimental conditions (e.g., the ionic strength of buffers), it is important to note that all these studies consistently indicate an enhancement in the membrane binding of hIIAPLA$_2$ upon the V3W mutation. Our results also indicate somewhat weaker binding of the F5W mutant of hIIAPLA$_2$ to anionic membranes. Although there are no published data to compare with this result, we interpret the impaired membrane binding of the F5W mutant in terms of its perturbed structure (see below).

Structure Assessment by Fluorescence and Circular Dichroism. To examine the structural effects of Trp mutations, fluorescence and far-UV CD spectra of hIIAPLA$_2$ and the two mutants were measured. Because hIIAPLA$_2$ has no tryptophans, its fluorescence spectrum was measured on the basis of tyrosine emission, using excitation at 275 nm, whereas for V3W and F5W mutants, tryptophan fluorescence spectra were measured using excitation at 290 nm. The fluorescence of hIIAPLA$_2$ had a peak at 306 nm, typical for Tyr emission spectra of folded proteins (*50*, *51*). Although no significant differences have been detected between the quantum yields of the Trp fluorescence of V3W and F5W mutants, emission peaks of Trp occurred at 347 and 331 nm for the V3W and F5W mutants, respectively (Figure 5A). The strongly blue shifted Trp fluorescence of the F5W compared to that of the V3W implies that Trp^5 is shielded from the aqueous phase inside the protein molecule, whereas Trp^3 is exposed to water and is involved in solvent relaxation.

The secondary structure of the proteins was assessed by far-UV CD. All three proteins displayed CD spectra with double minima around 208 and 222 nm and a peak around 192 nm (Figure 5B), indicating dominantly α-helical structure in all proteins (*52*, *53*). The general similarity of the three spectra of Figure 5B indicates that neither the V3W nor F5W mutations significantly perturbed the secondary structure of the protein. Baker et al. (*30*) observed little difference between the CD spectra of hIIAPLA$_2$ and the V3W mutant, consistent with our data.

Because PLA$_2$s are interfacially activated enzymes, it is of great interest to determine if the membrane binding of these proteins is accompanied by any conformational changes that may be related to enzyme activation. However, spectroscopic methods that operate in the ultraviolet region, such as far-UV CD and fluorescence, often encounter light scattering problems in the presence of relatively high

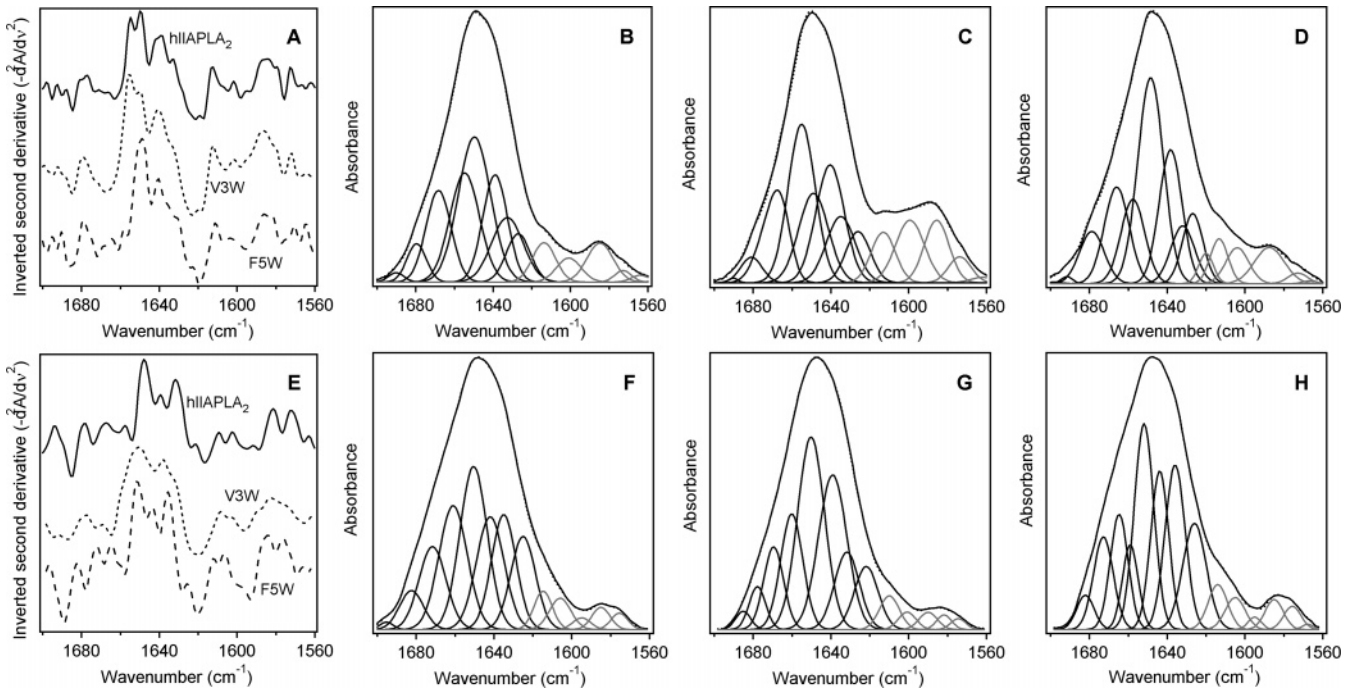

FIGURE 6: Inverted second derivative spectra of free (A) and membrane-bound (E) $hIIAPLA_2$ and the V3W and F5W mutants, as indicated. The curve-fitted spectra of the $hIIAPLA_2$ (B and F), the V3W mutant (C and G), and the F5W mutant (D and H) free in buffer (B, C, and D) and bound to supported membranes composed of 70 mol % POPC and 30 mol % POPG (F, G, and H). The components below 1620 cm^{-1}, which were not used for secondary structure characterization, are shown in light gray. In panels B, C, D, F, G, and H, the curve-fit, that is, the sum of all components, is shown as a dotted line and can hardly be discerned because it coincides with the experimental spectra, indicating good fitting. The buffer composition was 100 mM NaCl, 1 mM NaN_3, 1 mM EGTA, and 50 mM Hepes in D_2O at pH* 7.0.

concentrations of lipid vesicles. In this regard, FTIR spectroscopy offers a solution because of negligible light scattering in the infrared region. Moreover, the ATR-FTIR technique provides the spectra of membrane-bound proteins, unlike experiments on peripheral proteins in suspensions of lipid vesicles where the total signal contains contributions from both membrane-bound and free protein molecules. Therefore, we have used both direct transmission FTIR on free PLA_2s and ATR-FTIR on membrane-bound PLA_2s in order to assess the structural changes in $hIIAPLA_2$ and the Trp mutants upon membrane binding.

Structural Analysis by FTIR Spectroscopy. Information on the secondary and dynamic structural changes in $hIIAPLA_2$ and the mutants upon membrane binding was obtained by curve-fitting of the amide I bands of FTIR spectra of protein samples that were exposed to D_2O for 1 h. These spectra provide more information on the protein structure than those measured on proteins either dissolved in H_2O or exposed to D_2O for prolonged periods of time (*41*). Amide I curve-fitting was conducted using the component frequencies found from the second derivatives, as described previously (*41*, *42*). The inverted second derivatives identify multiple peaks in the spectral region 1700−1560 cm^{-1}, which were used for curve-fitting (Figure 6). In the amide I region, that is, between 1700 and 1620 cm^{-1}, which is sensitive to the protein backbone conformation, eight peaks were identified and used for characterization of the secondary structures of both free and membrane-bound proteins. Analysis of the FTIR data was performed on the basis of well-established assignments of amide I components to specific secondary structure types: components between 1660 and 1648 cm^{-1} were assigned to the α-helix; those between 1700 and 1660 cm^{-1} were assigned to β- and γ-turns and the high-frequency component of the antiparallel β-sheet; components between 1635 and 1625 cm^{-1} were assigned to the β-sheet structure; and the rest to irregular structures (*41*) and references therein).

The data summarized in Table 1 indicate two components in the α-helical region for all three proteins. For the $hIIAPLA_2$ and the V3W mutant free in buffer, these components are located around 1655 cm^{-1} and 1650−1649 cm^{-1}, which can be interpreted in terms of unexchanged and deuterated α-helices, respectively. This assignment results in 41−47% α-helix in both proteins, in agreement with high-resolution structures of group IIA PLA_2s (*54*, *55*). The data do not indicate major conformational changes caused by the V3W mutation, which agrees with the CD data (Figure 5). For these two proteins that are bound to supported membranes, the higher frequency α-helical component shifts to ~1661 cm^{-1}, while the other component undergoes little spectral shift. This may reflect structural destabilization of a fraction of α-helices during membrane binding, resulting in weaker helical H bonding, stronger backbone carbonyl bonds, and increased amide I frequencies, as detected earlier for a snake venom group IIA PLA_2 (*56*, *57*). In the case of $hIIAPLA_2$, the α-helical content appears to slightly decrease upon membrane binding, consistent with weaker helices in the membrane-bound PLA_2, whereas no such changes are observed for the V3W mutant.

Curve-fitting of the amide I bands of the F5W mutant yielded qualitatively different results. For both free and membrane-bound F5W mutants, two components were found in the conventional α-helical region, one around 1658 cm^{-1} and the other in the 1652−1648 cm^{-1} region, which are likely

Table 1: Amide I Band Components of Free and Membrane-bound hIIAPLA$_2$, the V3W Mutant, and the F5W Mutant, Determined by Curve Fitting of Spectra Obtained by Direct Transmission FTIR (for Free Proteins) and ATR-FTIR (for Membrane-Bound Proteins)

hIIAPLA$_2$				V3W-hIIAPLA$_2$				F5W-hIIAPLA$_2$			
free		membrane-bound		free		membrane-bound		free		membrane-bound	
ν, cm^{-1}	%	ν, cm^{-1}	%	ν, cm^{-1}	%	ν, cm^{-1}	%	ν, cm^{-1}	%	ν, cm^{-1}	%
1690.5	0.7	1695.3	0.6	1691.4	0.6	1684.7	1.7	1691.5	1.1	1681.8	2.8
1679.9	4.2	1682.7	4.7	1680.8	3.4	1677.9	3.7	1678.9	7.5	1673.1	10.4
1669.3	13.4	1671.2	11.5	1673.1	14.1	1669.3	9.1	1666.4	14.2	1664.4	11.3
1654.8	19.0	1660.6	18.1	1654.8	26.1	1660.6	14.0	1657.7	11.6	1658.6	7.4
1649.9	28.2	1650.9	22.8	1649.0	15.8	1649.9	28.5	1648.1	30.9	1651.9	20.7
1639.4	15.5	1642.3	16.1	1640.3	20.3	1639.4	23.9	1638.4	18.0	1644.2	15.8
1632.6	11.9	1634.5	14.3	1634.5	11.8	1631.6	10.7	1631.7	8.2	1635.5	18.0
1626.8	7.1	1624.9	11.9	1625.9	7.9	1622.0	8.4	1626.9	8.5	1625.8	13.6

to represent the α-helices with unexchanged and deuterated backbone amide groups. For the free protein, these components constitute 42.5% of the amide I band, which is similar to the helical content in the hIIAPLA$_2$ and the V3W mutant and implies that neither V3W nor F5W mutations cause significant structural changes in the free protein in buffer. However, for the membrane-bound F5W mutant, these two α-helical components constitute only 28% of the amide I band intensity, that is ∼14% less than that in the free protein. Interestingly, the fraction of components in the 1636−1626 cm^{-1} concomitantly increases by 15% upon membrane binding of the F5W mutant (Table 1). One presumptive interpretation of this result might be a conversion of 18 to 19 residues of the protein (15% of 124 residues) from α-helical conformation to *β*-structure. However, given the robust 3-D structure of secretory PLA$_2$s stabilized by multiple disulfides, this is very unlikely. Another, perhaps more reasonable interpretation of the amide I curve-fitting results is that upon membrane binding, the Trp^5 might tend to interact with the membrane because of the high affinity of Trp for the membrane−water interface (*25*, *26*), resulting in a structural distortion in the *N*-terminal region of the protein and the destabilization of the other two helices. The amide I component of the membrane-bound F5W at 1664 cm^{-1} may then be attributed to an α_{II}-type flexible helical structure (*58*) that absorbs in this infrared region (*59*−*61*). In this case, the total helical content of the membrane-bound F5W mutant would constitute 39.4%, that is, 3% (∼4 residues) less than the helical structure in the free protein. This result supports a conjecture that Trp^5 of the F5W mutant, which is located at the internal substrate-binding face of the *N*-terminal helix, tends to interact with the membrane and, thereby, cause a structural distortion of the first several residues of the protein upon membrane binding.

In light of these results, the decreased activity of the F5W mutant may be determined not by blockage of the substrate entrance into the active site slot but by a distorted *N*-terminal helix, which is known to be indispensable for PLA$_2$ activity (*23*). The fact that the activity of the F5W against zwitterionic phospholipid vesicles or micelles is almost completely lost but the mutant retains significant activity against anionic membranes (Figures 2 and 3) probably results from different modes of binding of the protein to zwitterionic or anionic interfaces. In the former case, tryptophan−membrane interactions are likely to play a significant role in protein binding to membranes, whereas in the latter case, the electrostatic interactions between the cationic face of the *N*-terminal helix and the anionic membrane determine effective membrane binding of PLA$_2$ without the involvement Trp. This is supported by the fact that group IB PLA$_2$s, which contain a Trp^3 at the membrane-binding surface, are active against zwitterionic membranes, unlike the highly cationic hIIAPLA$_2$, which has little activity against zwitterionic membranes but is very active against anionic membranes. Also, as shown in the accompanying article (*62*), Trp^3 of both human group IB PLA$_2$ and the V3W mutant of hIIAPLA$_2$ insert into membranes to a similar depth, suggesting that in both cases, Trp^3 facilitates PLA$_2$−membrane interaction by serving as a membrane anchor.

Dynamic Structural Changes Detected by FTIR Spectroscopy. One of the most powerful methods of probing protein dynamic structure is based on the analysis of amide HX kinetics, which can be measured by FTIR spectroscopy (*41*, *42*). The amide II band, which involves a major contribution from the amide N−H in-plane bending mode, shifts from ∼1545 to 1450 cm^{-1} upon amide deuteration, resulting in a time-dependent decrease in the intensity around 1545 cm^{-1}. Because each amide group in the protein has its individual exchange rate, depending upon solvent exposure, intramolecular H bonding, local sequence, and microenvironment, ideally the HX of a protein of n_{res} amino acid residues should be described using $n_{res} - 1$ rate constants (the number of peptide bonds). Although the multiexponential decay of the amide II intensity can be described by a large number of decay (rate) constants, this would not be a practically useful approach because with increasing numbers of fitting parameters the reliability of their values strongly decreases. Fitting the HX kinetics with three populations of amino acid residues, for example, exchange-resistant, slow-exchanging, and fast-exchanging populations, has been shown to be a reasonable approach because in most cases, the fractions and rate constants of these populations can be reliably determined (*41*, *42*).

We have employed this approach to characterize the changes in the dynamic structure of hIIAPLA$_2$ and the two Trp mutants induced by membrane binding. The data are shown in Figure 7, and the numerical parameters are summarized in Table 2. The data indicate an increase in the HX efficiency of all three molecules upon membrane binding, as clearly seen from Figure 7. Although in all three cases membrane binding results in a 5−10% decrease in the fraction of exchange-resistant amide groups a_0, the dynamic conformational changes in the F5W mutant are different from those occurring in hIIAPLA$_2$ and the V3W mutant. For the latter two proteins, membrane binding is accompanied by a decrease in a_0 and a_2 (the fractions of exchange-resistant and

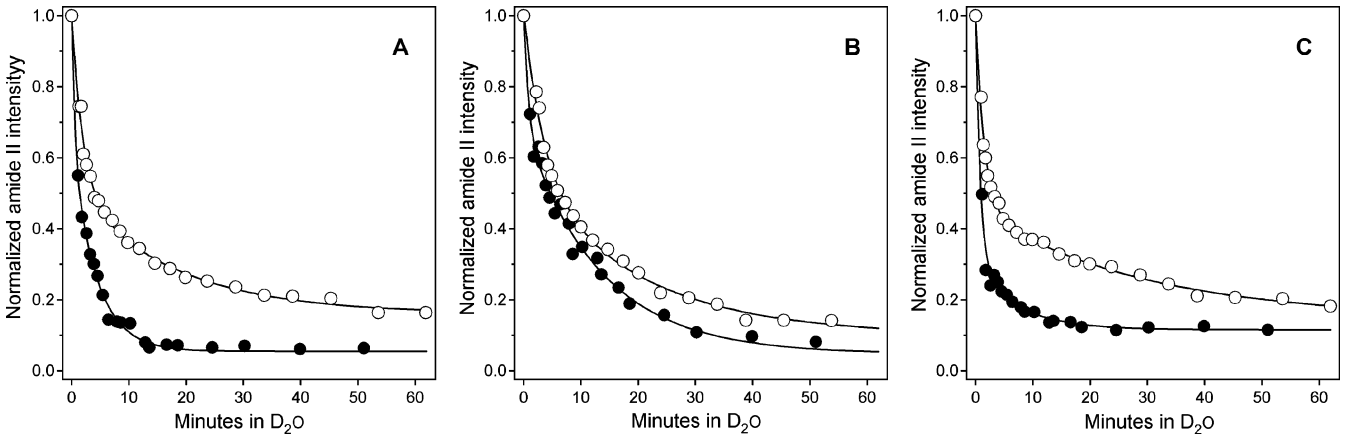

FIGURE 7: Kinetics of amide hydrogen/deuterium exchange of free and membrane-bound hIIAPLA$_2$ (A), the V3W mutant (B), and the F5W mutant (C), measured on the basis of the decrease in the integrated amide II band intensity upon exposure to D_2O. Data on free (○) and membrane-bound (●) proteins were obtained by direct transmission and ATR techniques, respectively. In the latter case, the spectra measured at parallel and perpendicular polarizations were used to obtain the corrected polarization-independent spectra, which were used for data analysis, as described in Materials and Methods/FTIR experiments. The supported membranes were composed of 70 mol % POPC and 30 mol % POPG. The buffer was, as specified in Figure 6, either in H_2O (at time zero) or in D_2O (at time $t > 0$). The lines were constructed through eq 4, using the best-fit parameters summarized in Table 2.

Table 2: Kinetic Parameters Characterizing the Amide Hydrogen/Deuterium Exchange of hIIAPLA$_2$, the V3W Mutant, and the F5W Mutant, Measured by Direct Transmission FTIR (for Free Proteins) and ATR-FTIR (for Membrane-Bound Proteins)

	hIIAPLA$_2$		V3W-hIIAPLA$_2$		F5W-hIIAPLA$_2$	
	free	membrane-bound	free	membrane-bound	free	membrane-bound
a_0	0.16	0.06	0.10	0.05	0.15	0.11
a_1	0.35	0.59	0.46	0.64	0.31	0.18
a_2	0.49	0.35	0.44	0.31	0.54	0.71
k_1 (min^{-1})	0.057	0.24	0.051	0.083	0.035	0.14
k_2 (min^{-1})	0.51	2.03	0.29	1.20	0.68	1.21

fast-exchanging amide groups) and an increase in the fraction of slow-exchanging amide groups a_1, with an increase in the rate constants of both slow- and fast-exchanging residues (k_1 and k_2, respectively). The decrease in a_0 and an overall increase in the rate constants of HX can be interpreted in a straightforward manner in terms of an increased motional flexibility of membrane-bound hIIAPLA$_2$ and the V3W mutant, consistent with the conclusion derived from the amide I curve-fitting data (Table 1). The increase in the fraction of slow-exchanging amide groups a_1, which is largely compensated by a decrease in the fraction of fast-exchanging groups a_2, most likely results from the seclusion of certain residues in the dehydrated protein−membrane interface and shielding from the solvent (note that the D_2O-based buffer was injected after protein binding to the supported membrane in an H_2O-based buffer). The decrease in a_2 upon membrane binding of the hIIAPLA$_2$ and the V3W mutant is 13−14%, indicating that approximately 17 amino acid residues, which undergo fast HX in the free protein, become less accessible to the solvent upon membrane binding. These are most likely the residues that constitute the membrane-binding face of the enzyme. Using an average accessible surface area of 200 Å^2 for amino acids (*63*) and assuming that nearly half of this area contributes to the protein surface area, we obtain ∼1700 Å^2 for the membrane-binding face of PLA_2, in good agreement with previous estimates (*11*).

The dynamic behavior of the F5W mutant is again different from those of hIIAPLA$_2$ and the V3W mutant. Membrane binding of the F5W mutant brings about a decrease in a_0 and a_1 and an increase in a_2. However, the rate constants of both slow- and fast-exchanging populations increase. The substantial increase in the fraction of the fast-exchanging residues, a_2, during the membrane binding of the F5W is in sharp contrast to the decrease in a_2 in the hIIAPLA$_2$ and the V3W mutant. Given the absence of dramatic differences in membrane-binding constants of all three proteins (Figure 4), this result implies that conformational destabilization of the F5W mutant during membrane binding, deduced from the amide I curve-fitting data (Figure 6 and Table 1), is probably significant enough to substantially increase the number of residues that rapidly undergo HX despite partial protection from the solvent by membrane binding. It is also possible that the mode of membrane binding of the F5W mutant is different from those of the hIIAPLA$_2$ and the V3W mutant, which was directly assessed by polarized ATR-FTIR spectroscopy, as described below.

Orientations of Membrane-Bound Proteins by Polarized ATR-FTIR Spectroscopy. Polarized ATR-FTIR spectroscopy was used to see if significant differences could be found between the orientations of membrane-bound hIIAPLA$_2$ and the two Trp mutants. The ratio of absorbance intensities at parallel and perpendicular polarizations of incident light yields the ATR dichroic ratio, $R^{ATR} = A_{\parallel}/A_{\perp}$, which is determined by the orthogonal components of the electric vector of the evanescent field, E_x, E_y, E_z, and the orientational order of the aligned sample. For an isotropic sample, the dichroic ratio is $R_{iso} = (E_x^2 + E_z^2)/E_y^2$, which yields $R_{iso} \approx 1.72$ for a lipid membrane supported on a germanium plate in an aqueous environment at an incidence angle of incoming light of $\gamma = 45°$ (*41*). If the effect of the lipid bilayer on the evanescent field is neglected, which may be justified because of its diminutive thickness (*64*), then $R_{iso} \approx 2.0$. This latter consideration is known as a two-phase approximation, whereas the one that takes the membrane refractive index into account is known as a three-phase approximation. For an α-helix, R^{ATR} values lower or higher than R_{iso} indicate

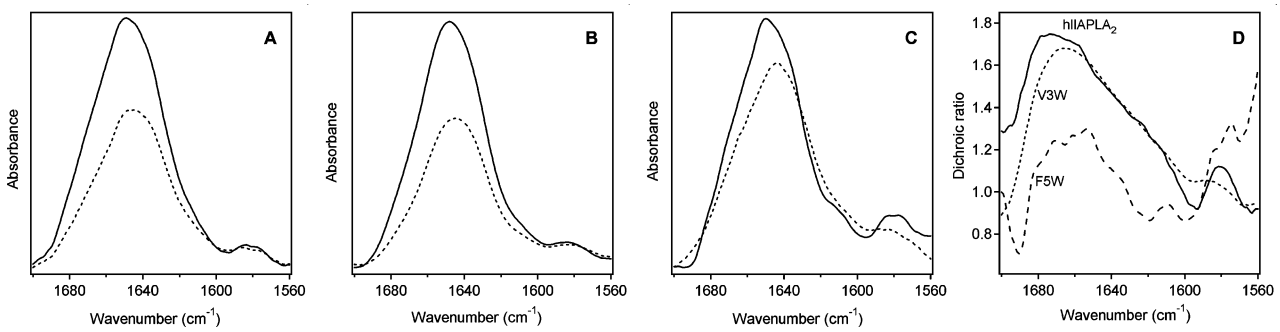

FIGURE 8: ATR-FTIR spectra of hIIAPLA$_2$ (A), the V3W mutant (B), and the F5W mutant (C) at parallel (—) and perpendicular (....) polarizations of the incident infrared light. The supported membrane and the buffer composition were the same as those in Figure 6. Panel D shows the dichroic spectra obtained by dividing the parallel spectra by the respective perpendicular spectra shown in panels A, B, and C.

horizontal or vertical orientation of the helix axis relative to the membrane plane, respectively. The physically meaningful limits of R^{ATR} are 1.3−3.6 and 1.4−4.5 for the three-phase and the two-phase approximations, respectively.

Spectra of the three proteins, bound to supported membranes composed of 70 mol % POPC and 30% POPG, were measured at parallel and perpendicular polarizations of incident light, as shown in Figure 8A, B, and C. These data show that the relative line shapes of the spectra are similar for hIIAPLA$_2$ and the V3W mutant (Figure 8A and B) but are significantly different for the F5W mutant (Figure 8C). To obtain information on the relative orientations of various secondary structure elements of the proteins, dichroic spectra were generated by dividing the parallel spectra by the perpendicular spectra and are shown in Figure 8D. The values of the dichroic ratios in each spectral region can be interpreted in terms of spatial orientation of the corresponding secondary structure. Here, we will only consider the helical orientations because the α-helix is the predominant secondary structure in hIIAPLA$_2$ and is well characterized in terms of polarized ATR-FTIR. In the α-helical region, the R^{ATR} is 1.58−1.65 for hIIAPLA$_2$ and 1.60−1.63 for the V3W mutant. Because these are the weight-averaged dichroic ratios generated by at least three different α-helices in each protein, they cannot be interpreted in terms of helical orientation in a straightforward way. However, the fact that the values are below R_{iso}, for both three- and two-phase approximations, indicates that the helices are closer to a horizontal orientation, that is, they are strongly inclined toward the membrane surface. This is consistent with the orientation of the structurally similar human IB PLA$_2$, which is oriented in such a way that the helices are tilted from the membrane normal by 70−80° (*19*, *23*), and also agrees with the orientation of hIIAPLA$_2$ on mixed phospholipid/surfactant micelles (*46*).

The dichroic spectrum of the F5W mutant strongly deviates from those of hIIAPLA$_2$ and the V3W mutant; the R^{ATR} is ∼1.3 in the α-helical region (Figure 8D). This indicates that the helices of the F5W mutant lie nearly parallel to the membrane surface. The fact that the value of R^{ATR} is beyond the lower limit set by the two-phase approximation for an α-helix, may also indicate a distortion of the helical structure in the F5W mutant during membrane binding. Altogether, these data clearly indicate that although hIIAPLA$_2$ and the V3W mutant adopt similar and apparently productive mode orientations at the membrane surface, the orientation of the F5W mutant is significantly different, and probably, the helices of the latter protein undergo distortion during membrane binding. This conclusion is in accordance with the above findings that the membrane binding of the F5W mutant results in significant conformational changes, involving distortion of the helical structure at the *N*-terminus. These conformational changes likely occur because of the tendency of Trp to interact with the membrane and exert an inhibitory effect on the enzyme. In contrast, the membrane binding of hIIAPLA$_2$ and the V3W mutant only causes an increase in flexibility, but not distortion, of the helical structure.

CONCLUSIONS

The major finding of this work is the dramatic structural and functional differences between two hIIAPLA$_2$ mutants in which a Trp is introduced into closely located positions 3 or 5. Although the V3W mutant demonstrates enhanced activity compared to that of hIIAPLA$_2$, the F5W mutant has negligible activity against PC membranes or micelles but shows considerable activity against anionic membranes. The reason for these activity differences does not lie in the different membrane-binding affinities of the proteins because all three molecules have comparable dissociation constants for POPC/POPG membranes. Although far-UV CD data show little differences in the secondary structures of free proteins in buffer, ATR-FTIR data reveal large conformational differences between the membrane-bound proteins. Membrane binding of the F5W mutant results in the distortion of several helical residues and probably a α_I-to-α_{II} helical transition, which may be caused by a tendency of Trp^5 to interact with the membrane surface upon membrane binding of the protein. This is a viable mechanism because the energy of the Trp−membrane interaction (approximately −3 kcal/mol (*65*)) is comparable to the energy of helical H bonding. Data on the amide HX kinetics support the conclusion on a membrane-induced structural destabilization of the F5W protein. Finally, the angular orientations of membrane-bound hIIAPLA$_2$ and the V3W are similar and consistent with available data, whereas the disparate orientation of the F5W mutant is indicative of a disturbed conformation. The data are consistent with a mechanism suggesting that the suppression of the PLA$_2$ activity by the F5W mutation results from conformational perturbation of the enzyme during membrane binding rather than a blockage of the active site slot, as might be expected. Our results of dramatically different structural and functional effects of Trp mutations at two closely positioned sites of PLA$_2$ demonstrate

how efficiently enzyme function can be modulated by targeted protein engineering.

ACKNOWLEDGMENT

We are grateful to Professor David C. Wilton of the University of Southampton for the kind gift of the hIIAPLA$_2$ expression plasmid and Professor Jeffrey L. Urbauer of the University of Georgia for his help at the initial stages of this work.

REFERENCES

1. Balsinde, J., Winstead, M. V., and Dennis, E. A. (2002) Phospholipase A_2 regulation of arachidonic acid mobilization, *FEBS Lett. 531*, 2−6.
2. Dennis, E. A. (2000) Phospholipase A_2 in eicosanoid generation, *Am. J. Respir. Crit. Care Med. 161*, S32−S35.
3. Gilroy, D. W., Newson, J., Sawmynaden, P., Willoughby, D. A., and Croxtall, J. D. (2004) A novel role for phospholipase A_2 isoforms in the checkpoint control of acute inflammation, *FASEB J. 18*, 489−498.
4. Granata, F., Balestrieri, B., Petraroli, A., Giannattasio, G., Marone, G., and Triggiani, M. (2003) Secretory phospholipases A_2 as multivalent mediators of inflammatory and allergic disorders, *Int. Arch. Allergy Immunol. 131*, 153−163.
5. Murakami, M., and Kudo, I. (2004) Secretory phospholipase A_2, *Biol. Pharm. Bull. 27*, 1158−1164.
6. Beers, S. A., Buckland, A. G., Koduri, R. S., Cho, W, Gelb, M. H., and Wilton, D. C. (2002) The antibacterial properties of secreted phospholipases A_2: a major physiological role for the group IIA enzyme that depends on the very high pI of the enzyme to allow penetration of the bacterial cell wall, *J. Biol. Chem. 277*, 1788−1793.
7. Buckland, A. G., and Wilton, D. C. (2000) The antibacterial properties of secreted phospholipases A_2, *Biochim. Biophys. Acta 1488*, 71−82.
8. Webb, N. R. (2005) Secretory phospholipase A_2 enzymes in atherogenesis, *Curr. Opin. Lipidol. 16*, 341−344.
9. Donato, N. J., Martin, C. A., Perez, M., Newman, R. A., Vidal, J. C., and Etcheverry, M. (1996) Regulation of epidermal growth factor receptor activity by crotoxin, a snake venom phospholipase A_2 toxin. A novel growth inhibitory mechanism, *Biochem. Pharmacol. 51*, 1535−1543.
10. Yamazaki, Y., Matsunaga, Y., Nakano, Y., and Morita, T. (2005) Identification of vascular endothelial growth factor receptor-binding protein in the venom of eastern cottonmouth. A new role of snake venom myotoxic Lys49-phospholipase A_2, *J. Biol. Chem. 280*, 29989−29992.
11. Berg, O. G., Gelb, M. H., Tsai, M. D., and Jai, M. K. (2001) Interfacial enzymology: the secreted phospholipase A_2-paradigm, *Chem. Rev. 101*, 2613−2654.
12. Scott, D. L., and Sigler, P. B. (1994) Structure and catalytic mechanism of secretory phospholipases A_2, *Adv. Protein Chem. 45*, 53−88.
13. Apitz-Castro, R., Jain, M. K., and de Haas, G. H. (1982) Origin of the latency phase during the action of phospholipase A_2 on unmodified phosphatidylcholine vesicles, *Biochim. Biophys. Acta 688*, 349−356.
14. Berg, O. G., Rogers, J., Yu, B.-Z., Yao, J., Romsted, L. S., and Jain, M. K. (1997) Thermodynamic and kinetic basis of interfacial activation: resolution of binding and allosteric effects on pancreatic phospholipase A_2 at zwitterionic interfaces, *Biochemistry 36*, 14512−14530.
15. Berg, O. G., Yu, B.-Z., Rogers, J., and Jain, M. K. (1991) Interfacial catalysis by phospholipase A_2: determination of the interfacial kinetic rate constants, *Biochemistry 30*, 7283−7297.
16. Bezzine, S., Bollinger, J. G., Singer, A. G., Veatch, S. L., Keller, S. L., and Gelb, M. H. (2002) On the binding preference of human groups IIA and X phospholipases A_2 for membranes with anionic phospholipids, *J. Biol. Chem. 277*, 48523−48534.
17. Gadd, M. E., and Biltonen, R. L. (2000) Characterization of the interaction of phospholipase A_2 with phosphatidylcholine-phosphatidylglycerol mixed lipids, *Biochemistry 39*, 9623−9631.
18. Bahnson, B. J. (2005) Structure, function and interfacial allosterism in phospholipase A_2: insight from the anion-assisted dimer, *Arch. Biochem. Biophys. 433*, 96−106.
19. Qin, S., Pande, A. H., Nemec, K. N., He, X., and Tatulian, S. A. (2005) Evidence for the regulatory role of the N-terminal helix of secretory phospholipase A_2 from studies on native and chimeric proteins, *J. Biol. Chem. 280*, 36773−36783.
20. Yu, B.-Z., Rogers, J., Tsai, M. D., Pidgeon, C., and Jain, M. K. (1999) Contributions of residues of pancreatic phospholipase A_2 to interfacial binding, catalysis, and activation, *Biochemistry 38*, 4875−4884.
21. Liu, X., Zhu, H., Huang, B., Rogers, J., Yu, B.-Z., Kumar, A., Jain, M. K., Sundaralingam, M., and Tsai, M. D. (1995) Phospholipase A_2 engineering. Probing the structural and functional roles of N-terminal residues with site-directed mutagenesis, X-ray, and NMR, *Biochemistry 34*, 7322−7334.
22. Othman, R., Baker, S., Li, Y., Worrall, A. F., and Wilton, D. C. (1996) Human nonpancreatic (group II) secreted phospholipase A_2 expressed from a synthetic gene in *Escherichia coli*: characterisation of N-terminal mutants, *Biochim. Biophys. Acta 1303*, 92−102.
23. Qin, S., Pande, A. H., Nemec, K. N., and Tatulian, S. A. (2004) The N-terminal α-helix of pancreatic phospholipase A_2 determines productive-mode orientation of the enzyme at the membrane surface, *J. Mol. Biol. 344*, 71−89.
24. Snitko, Y., Koduri, R. S., Han, S. K., Othman, R., Baker, S. F., Molini, B. J., Wilton, D. C., Gelb, M. H., and Cho, W. (1997) Mapping the interfacial binding surface of human secretory group IIa phospholipase A_2, *Biochemistry 36*, 14325−14333.
25. Clark, E. H., East, J. M., and Lee, A. G. (2003) The role of tryptophan residues in an integral membrane protein: diacylglycerol kinase, *Biochemistry 42*, 11065−11073.
26. Yau, W. M., Wimley, W. C., Gawrisch, K., and White, S. H. (1998) The preference of tryptophan for membrane interfaces, *Biochemistry 37*, 14713−14718.
27. Angulo, Y., Olamendi-Portugal, T., Alape-Giron, A., Possani, L. D., and Lomonte, B. (2002) Structural characterization and phylogenetic relationships of myotoxin II from *Atropoides* (*Bothrops*) *nummifer* snake venom, a Lys49 phospholipase A_2 homologue, *Int. J. Biochem. Cell Biol. 34*, 1268−1278.
28. de Sousa, M. V., Morhy, L., Arni, R. K., Ward, R. J., Diaz, C., and Gutierrez, J. M. (1998) Amino acid sequence of a myotoxic Lys49-phospholipase A_2 homologue from the venom of *Cerrophidion* (*Bothrops*) *godmani*, *Biochim. Biophys. Acta 1384*, 204−208.
29. Tsai, I. H., Wang, Y. M., Au, L. C., Ko, T. P., Chen, Y. H., and Chu, Y. F. (2000) Phospholipases A_2 from *Callosellasma rhodostoma* venom gland cloning and sequencing of 10 of the cDNAs, three-dimensional modelling and chemical modification of the major isozyme, *Eur. J. Biochem. 267*, 6684−6691.
30. Baker, S. F., Othman, R., and Wilton, D. C. (1998) Tryptophan-containing mutant of human (group IIa) secreted phospholipase A_2 has a dramatically increased ability to hydrolyze phosphatidylcholine vesicles and cell membranes, *Biochemistry 37*, 13203−13211.
31. Beers, S. A., Buckland, A. G., Giles, N., Gelb, M. H., and Wilton, D. C. (2003) Effect of tryptophan insertions on the properties of the human group IIA phospholipase A_2: mutagenesis produces an enzyme with characteristics similar to those of the human group V phospholipase A_2, *Biochemistry 42*, 7326−7338.
32. Cha, S. S., Lee, D., Adams, J., Kurdyla, J. T., Jones, C. S., Marshall, L. A., Bolognese, B., Abdel-Meguid, S. S., and Oh, B. H. (1996) High-resolution X-ray crystallography reveals precise binding interactions between human nonpancreatic secreted phospholipase A_2 and a highly potent inhibitor (FPL67047XX), *J. Med. Chem. 39*, 3878−3881.
33. Hansford, K. A., Reid, R. C., Clark, C. I., Tyndall, J. D., Whitehouse, M. W., Guthrie, T., McGeary, R. P., Schafer, K., Martin, J. L., and Fairlie, D. P. (2003) D-Tyrosine as a chiral precursor to potent inhibitors of human nonpancreatic secretory phospholipase A_2 (IIa) with antiinflammatory activity, *ChemBioChem 4*, 181−185.
34. Plesniak, L. A., Yu, L., and Dennis, E. A. (1995) Conformation of micellar phospholipid bound to the active site of phospholipase A_2, *Biochemistry 34*, 4943−4951.
35. van den Berg, B., Tessari, M., Boelens, R., Dijkman, R., Kaptein, R., de Haas, G. H., and Verheij, H. M. (1995) Solution structure of porcine pancreatic phospholipase A_2 complexed with micelles and a competitive inhibitor, *J. Biomol. NMR 5*, 110−121.
36. Lakowicz, J. R. (1999) *Principles of Fluorescence Spectroscopy*, 2nd ed., Kluwer Academic/Plenum Publishers, New York.

37. Golding, C., Senior, S., Wilson, M. T., and O'Shea, P. (1996) Time resolution of binding and membrane insertion of a mitochondrial signal peptide: Correlation with structural changes and evidence for cooperativity, *Biochemistry 35*, 10931−10937.
38. Wall, J., Golding, C. A., Van Veen, M., and O'Shea, P. (1995) The use of fluoresceinphosphatidylethanolamine (FPE) as a real-time probe for peptide-membrane interactions, *Mol. Membr. Biol. 12*, 183−192.
39. Pande, A. H., Qin, S., and Tatulian, S. A. (2005) Membrane fluidity is a key modulator of membrane binding, insertion, and activity of 5-lipoxygenase, *Biophys. J. 88*, 4084−4094.
40. Marsh, D. (1999) Quantitation of secondary structure in ATR infrared spectroscopy, *Biophys. J. 77*, 2630−2637.
41. Tatulian, S. A. (2003) Attenuated total reflection Fourier transform infrared spectroscopy: A method of choice for studying membrane proteins and lipids, *Biochemistry 42*, 11898−11907.
42. Tatulian, S. A., Cortes, D. M., and Perozo, E. (1998) Structural dynamics of the *Streptomyces lividans* K^+ channel (SKC1): secondary structure characterization from FTIR spectroscopy, *FEBS Lett. 423*, 205−212.
43. Bayburt, T., Yu, B.-Z., Lin, H. K., Browning, J., Jain, M. K., and Gelb, M. H. (1993) Human nonpancreatic secreted phospholipase A_2: interfacial parameters, substrate specificities, and competitive inhibitors, *Biochemistry 32*, 573−582.
44. Hønger, T., Jorgensen, K., Stokes, D., Biltonen, R. L., and Mouritsen, O. G. (1997) Phospholipase A_2 activity and physical properties of lipid-bilayer substrates, *Methods Enzymol. 286*, 168−190.
45. Burack, W. R., Gadd, M. E., and Biltonen, R. L. (1995) Modulation of phospholipase A_2: identification of an inactive membrane-bound state, *Biochemistry 34*, 14819−14828.
46. Canaan, S., Nielsen, R., Ghomashchi, F., Robinson, B. H., and Gelb, M. H. (2002) Unusual mode of binding of human group IIA secreted phospholipase A_2 to anionic interfaces as studied by continuous wave and time domain electron paramagnetic resonance spectroscopy, *J. Biol. Chem. 277*, 30984−30990.
47. Diraviyam, K., and Murray, D. (2006) Computational analysis of the membrane association of group IIA secreted phospholipases A_2: a differential role for electrostatics, *Biochemistry 45*, 2584−2598.
48. Tatulian, S. A. (2002) Quantitative characterization of membrane binding of peripheral proteins by spin-label EPR spectroscopy, *J. Phys. Chem. B 106*, 8870−8877.
49. Gelb, M. H., Cho, W., and Wilton, D. C. (1999) Interfacial binding of secreted phospholipases A_2: more than electrostatics and a major role for tryptophan, *Curr. Opin. Struct. Biol. 9*, 428−432.
50. Donato, H., Jr., Mani, R. S., and Kay, C. M. (1991) Spectral studies on the cadmium-ion-binding properties of bovine brain S-100b protein, *Biochem. J. 276*, 13−18.
51. Ruan, K., Li, J., Liang, R., Xu, C., Yu, Y., Lange, R., and Balny, C. (2002) A rare protein fluorescence behavior where the emission is dominated by tyrosine: case of the 33-kDa protein from spinach photosystem II, *Biochem. Biophys. Res. Commun. 293*, 593−597.
52. Sreerama, N., and Woody R. W. (2000) Circular Dichroism of Peptides and Proteins, in *Circular Dichroism: Principles and Applications* (Berova, N., Nakanishi, K., and Woody, R. W., Eds.) 2nd ed., pp 601−620, Wiley-VCH, New York.
53. Woody, R. W., and Dunker, A. K. (1996) Aromatic and Cysteine Side-Chain Circular Dichroism in Proteins, in *Circular Dichroism and the Conformational Analysis of Biomolecules* (Fasman, G. D., Ed.), pp 109−157, Plenum Press, New York and London.
54. Edwards, S. H., Thompson, D., Baker, S. F., Wood, S. P., and Wilton, D. C. (2002) The crystal structure of the H48Q active site mutant of human group IIA secreted phospholipase A_2 at 1.5 Å resolution provides an insight into the catalytic mechanism, *Biochemistry 41*, 15468−15476.
55. Scott, D. L., White, S. P., Browning, J. L., Rosa, J. J., Gelb, M. H., and Sigler, P. B. (1991) Structures of free and inhibited human secretory phospholipase A_2 from inflammatory exudate, *Science 254*, 1007−1010.
56. Tatulian, S. A. (2001) Toward understanding interfacial activation of secretory phospholipase A_2 (PLA_2): membrane surface properties and membrane-induced structural changes in the enzyme contribute synergistically to PLA_2 activation, *Biophys. J. 80*, 789−800.
57. Tatulian, S. A., Biltonen, R. L., and Tamm, L. K. (1997) Structural changes in a secretory phospholipase A_2 induced by membrane binding: a clue to interfacial activation? *J. Mol. Biol. 268*, 809−815.
58. Némethy, G., Phillips, D. C., Leach, S. J., and Scheraga, H. A. (1967) A second right-handed helical structure with the parameters of the Pauling-Corey α-helix, *Nature 214*, 363−365.
59. Barnett, S. M., Edwards, C. M., Butler, I. S., and Levin, I. W. (1997) Pressure-induced transmembrane α_{II} to α_I-helical conversion in bacteriorhodopsin: An infrared spectroscopic study, *J. Phys. Chem. B 101*, 9421−9424.
60. Dwivedi, A. M., and Krimm, S. (1984) Vibrational analysis of peptides, polypeptides, and proteins. XVIII. Conformational sensitivity of the alpha-helix spectrum: α_I- and α_{II}-poly(L-alanine), *Biopolymers 23*, 923−943.
61. Rothschild, K. J., and Clark, N. A. (1979) Anomalous amide I infrared absorption of purple membrane, *Science 204*, 311−312.
62. Pande, A. H., Qin, S., Nemec, K. N., and Tatulian, S. A. (2006) Isoform-specific membrane insertion of secretory phospholipase A_2 and functional implications, *Biochemistry*, *45*, pp 12436-12447.
63. Chothia, C. (1976) The nature of the accessible and buried surfaces in proteins, *J. Mol. Biol. 105*, 1−12.
64. Axelsen, P. H., and Citra, M. J. (1996) Orientational order determination by internal reflection infrared spectroscopy, *Prog. Biophys. Mol. Biol. 66*, 227−253.
65. White, S. H., and Wimley, W. C. (1999) Membrane protein folding and stability: physical principles, *Annu. Rev. Biophys. Biomol. Struct. 28*, 319−365.

BI061440R